**xxxxx manuscript No.**
(will be inserted by the editor)

# Constraints on $\sigma_8$ degeneracies from linear Nash-Greene perturbations in subhorizon scale[a]

**Abraão J. S. Capistrano**[a,1]

[1]Federal University of Latin-American Integration, 85867-970, Foz do Iguaçu-PR, Brazil.

Received: date / Accepted: date

**Abstract** Using a joint statistical analysis, we test a four-dimensional FLWR model embedded in a five-dimensional bulk based on the Nash-Greene embedding theorem. Performing a Markov Chain Monte Carlo (MCMC) modelling, we combine observational data sets as those of the recent "Gold 2018" growth data, the best-fit Planck2018/$\Lambda$CDM parameters on the Cosmic Microwave Background (CMB), the Baryon Acoustic Oscillations (BAO) measurements, the Pantheon Supernovae type Ia and the Hubble parameter data with redshift ranging from $0.01 < z < 2.3$ to impose restrictions on the model. From linear Nash-Green fluctuations of the metric, we obtain the related perturbed equations in longitudinal Newtonian gauge to obtain the evolution of growth matter. We show that a mild alleviation is obtained from the $\sigma$ tension between the growth amplitude factor and the matter content $(\sigma_8\text{-}\Omega_m)$ of the observations from CMB and Large Scale Structure (LSS) probes with degeneracies on the parameters. We also apply the Om(z) diagnosis to distinguish the model from $\Lambda$CDM. The Akaike Information Criterion (AIC) is used and we find a relative statistical consistence of the present model with both $\Lambda$CDM and $w$CDM models up to 1% of percentage difference at early times.

## 1 Introduction

The true mechanism behind the accelerated phase of the universe still remains an open question. After more than 20 years since the very first evidences of the cosmic accelerated expansion, one of the pivotal directions of investigations is about to unravel whether the dark energy equation of state (EoS), with the main fluid parameter $w(z)$, is restricted to the value $w_0 = -1$, as suggested by observations [1, 2], in conformity with the very popular $\Lambda$CDM model, or if there exists any deviations from that value leading to dynamical dark energy models. Even though its success, the $\Lambda$CDM model lacks of an underlying physical understanding, since the Cosmological constant $\Lambda$ and the Cold dark matter (CDM) are problems of their own nature [3–9].

The theoretical background of this paper relies on the possibility that the universe may be embedded in a larger space and the dark energy problem may be explained as a geometric outcome from the extrinsic curvature to amplify the gravitational strength of Einstein's gravity. Most of these extra dimensional models have been Kaluza-Klein or/and string inspired, such as, for instance, the Arkani-Hamed, Dvali and Dimopolous (ADD) model [10], the Randall-Sundrum model [11, 12] and the Dvali-Gabadadze-Porrati model (DPG) [13] commonly referred as braneworld models. Differently form these models and variants, we investigate how the embedding regarded as a prior mathematical structure can be suited for construction of a physical theory, keeping no relation with brane or string proposals. Several authors have been explored this possibility in many contexts [14–30]. Moreover, a cosmological model is proposed based on previous works at background level [16, 20, 23, 24] and we proceed further to obtain the cosmological perturbed equations to be discussed in section 3.

This paper aims at investigating the $\sigma_8$ tension revealed by the notorious cryptic discrepancy of the data inferred from Planck CMB radiation and the Large Scale Structure (LSS) observations with the $\Lambda$CDM model as a background, and possibly explanations may come from modified gravity [31–37]. The $\sigma_8$ denotes the r.m.s amplitude of matter density at a scale of a radius $R \sim 8\text{h.Mpc}^{-1}$ within a enclosed mass of a sphere. We perform the Markov Chain Monte Carlo (MCMC) sample technique with a modified code from [38, 39] using the joint likelihood of kinematical probes as of the Cosmic Microwave Background (CMB) Planck2015 [1] and Planck2018 [2] datasets, the largest dataset Pantheon SnIa [40] with redshift ranging from $0.01 < z < 2.3$ that

[a]e-mail: abecapistrano@gmail.com

guarantees a low and intermediate redshift data, the Hubble parameter as a function of redshift $H(z)$ [41–46] and Baryonic Acoustic Oscillations (BAO) from points of the joint surveys 6dFGS [47], SDDS [48], BOSS CMASS [49], WiggleZ [50], MSG [51] and BOSS DR12 [52]. A comparison with the $\Lambda$CDM and general relativity (GR) quintessense ($w$CDM) [53, 54] is presented with analysis on the growth density evolution and Om(z) diagnosis [55]. In addition, we apply the Akaike Information Criterion [56] on the resulting contours confidence regions. In the final section, we conclude with our final remarks and prospects.

## 2 The theoretical framework

### 2.1 The D-dimensional equations

We start with a summary of main elements of a gravitational model based on the mathematical background of the theory of dynamical embeddings [15–17]. The first mechanism is the defined by the gravitational action functional. Thus, in the presence of confined matter fields on a four-dimensional space with thickness $l$ embedded in a D-dimensional ambient space (bulk), we define

$$S = -\frac{1}{2\kappa_D^2}\int \sqrt{|\mathcal{G}|}\mathcal{R}d^Dx - \int \sqrt{|\mathcal{G}|}\mathcal{L}_m^* d^Dx\,, \tag{1}$$

where $\kappa_D^2$ is the fundamental energy scale on the embedded space, $\mathcal{R}$ denotes the Ricci scalar of the bulk and $\mathcal{L}_m^*$ is the confined matter lagrangian. The normal radii $l$ is the smallest value of the curvature radii obtained from the relation

$$det(g_{\mu\nu} - l^a k_{\mu\nu a}) = 0\,. \tag{2}$$

In a geometrical sense, the term $l^a$ represents a displacement of the embedded space along the extra-dimensions.

The matter energy momentum tensor occupies a finite hypervolume with constant radius $l$ along the extra-dimensions. The variation of Einstein-Hilbert action in Eq.(1) with respect to the bulk metric $\mathcal{G}_{AB}$ leads to the Einstein equations for the bulk

$$\mathcal{R}_{AB} - \frac{1}{2}\mathcal{G}_{AB} = \alpha^\star\,\mathcal{T}_{AB}\,, \tag{3}$$

where $\alpha^\star = 8\pi G^*$ is energy scale parameter and $G^*$ is the bulk "gravitational constant". The tensor $\mathcal{T}_{AB}$ is the energy-momentum tensor for the bulk [16, 17, 20]. To generate a thick embedded space-time is important to perturb the related background and can be done using the confinement hypothesis that depends only on the four-dimensionality of the space-time [58–60], even though any gauge theory can be mathematically constructed in a higher dimensional space.

In order to obtain a more general theory based on embeddings to elaborate a physical model, Nash's original embedding theorem [61] used a flat D-dimensional Euclidean space, later generalized to any Riemannian manifold including non-positive signatures by Greene [62] with independent orthogonal perturbations. This choice of perturbations facilitates to obtain a differentiable smoothness of the embedding between the manifolds, which is a primary concern of Nash's theorem and satisfies the Einstein-Hilbert principle, where the variation of the Ricci scalar is the minimum as possible. Accordingly, it guarantees that the embedded geometry remains smooth (differentiable) after smooth (differentiable) perturbations.

With all these concepts, let us consider a Riemannian geometry $V_4$ with a non-perturbed metric $\bar{g}_{\mu\nu}$ being locally and isometrically embedded in a D-dimensional Riemannian geometry $V_n$. The embedded space-time $V_4$ is endowed with the local coordinates $x^\mu = \{x^0,...,x^3\}$ whereas the extra-dimensions in the bulk space can be defined with the coordinates $x^a = \{x^4,...,x^{D-1}\}$ and $D = 4+n$. Hence, the bulk local coordinates can be denoted by the set $\{x^\mu, x^a\}$. All these definitions allow us to construct a differentiable and regular map $\mathcal{X} : V_4 \to V_n$ satisfying the embedding equations

$$\mathcal{X}^A_{,\mu}\,\mathcal{X}^B_{,\nu}\mathcal{G}_{AB} = \bar{g}_{\mu\nu}\ , \tag{4}$$

$$\mathcal{X}^A_{,\mu}\,\bar{\eta}^B_a\mathcal{G}_{AB} = 0\ , \tag{5}$$

$$\bar{\eta}^A_a\,\bar{\eta}^B_b\mathcal{G}_{AB} = \bar{g}_{ab}\ , \tag{6}$$

where the set of $\mathcal{X}^A(x^\mu, x^a) : \mathcal{X}^A = \{\mathcal{X}^0...\mathcal{X}^{D-1}\}$ denotes the non-perturbed embedding function coordinates, the metric $\mathcal{G}_{AB}$ denotes the metric components of $V_D$ in arbitrary coordinates and $\bar{\eta}^A_a$ denotes a non-perturbed unit vector field orthogonal to $V_4$. Concerning notation, capital Latin indices run from 1 to $n$. Small case Latin indices refer to the extra dimension considered. All Greek indices refer to the embedded space-time counting from 1 to 4. Those sets of equations represent, respectively, the isometry condition in Eq.(4), the orthogonality between the embedding coordinates $\mathcal{X}$ and $\bar{\eta}$ in Eq.(5), and also, the vector normalization $\bar{\eta}^A_a$ and $\bar{g}_{ab} = \varepsilon_a\delta_{ab}$ with $\varepsilon_a = \pm 1$ in which the signs represent the signatures of the extra-dimensions. Hence, the integration of the system of equations Eqs.(4), (5) and (6) assures a correct configuration of the embedding map $\mathcal{X}$.

The non-perturbed extrinsic curvature $\bar{k}_{\mu\nu}$ of $V_4$ is, by definition, the projection of the variation of $\bar{\eta}$ onto the tangent plane :

$$\bar{k}_{\mu\nu} = -\mathcal{X}^A_{,\mu}\bar{\eta}^B_{,\nu}\mathcal{G}_{AB} = \mathcal{X}^A_{,\mu\nu}\bar{\eta}^B\mathcal{G}_{AB}\,, \tag{7}$$

where the comma denotes the ordinary derivative.

If one defines a geometric object $\bar{\omega}$ in $V_4$, its Lie flow for a small distance $\delta y$ is given by $\Omega = \bar{\Omega} + \delta y \pounds_{\bar{\eta}}\bar{\Omega}$, where $\pounds_{\bar{\eta}}$ denotes the Lie derivative with respect to $\bar{\eta}$. In particular, the Lie transport of the Gaussian veilbein $\{\mathcal{X}^A_\mu, \bar{\eta}^A_a\}$, defined on $V_4$ gives straightforwardly the perturbed coordinate $\mathcal{Z}^A(x^\mu, y^a) := \mathcal{Z}^A$ such as

$$\mathcal{Z}^A_{,\mu} = X^A_{,\mu} + \delta y^a\,\pounds_{\bar{\eta}}X^A_{,\mu} = \mathcal{X}^A_{,\mu} + \delta y^a\,\bar{\eta}^A_{a,\mu}\,, \tag{8}$$

$$\eta^A_a = \bar{\eta}^A_a + \delta y^b\,[\bar{\eta}_a, \bar{\eta}_b]^A = \bar{\eta}^A_a\,. \tag{9}$$

It is worth mentioning that Eq.(9) shows that the normal vector $\eta^A$ does not change under orthogonal perturbations. However, from Eq.(7), we note that in general $\eta_{,\mu} \neq \bar{\eta}_{,\mu}$. Hence, to describe the perturbed embedded geometry, we set a perturbed coordinates $\mathscr{Z}^A$ that are needed to satisfy the embedding equations similar to Eqs.(4), (5) and (6) as

$$\mathscr{Z}^A_{,\mu} Z^B_{,\nu} \mathscr{G}_{AB} = g_{\mu\nu},\ \mathscr{Z}^A_{,\mu} \eta^B_b \mathscr{G}_{AB} = g_{\mu b},\ \eta^A_a \eta^B_b, \mathscr{G}_{AB} = g_{ab}\ , \quad (10)$$

where $g_{ab} = \varepsilon_a \delta_{ab}$ with $\varepsilon_a = \pm 1$.

If we take Eq.(10) and rewrite Eq.(5) as

$$g_{\mu b} = \mathscr{Z}^A_{,\mu} \eta^B_b \mathscr{G}_{AB} = \delta y^a A_{\mu ab}\ . \quad (11)$$

Then, Eq.(11) results from a generalization of the Gauss-Weingarten equations

$$\eta^A_{a,\mu} = A_{\mu ac} g^{cb} \eta^A_b - \bar{k}_{\mu\rho a} \bar{g}^{\rho\nu} \mathscr{Z}^A_{,\nu}\ , \quad (12)$$

that leads to

$$A_{\mu ab} = \eta^A_{a,\mu} \eta^B_b \mathscr{G}_{AB} = \bar{\eta}^A_{a,\mu} \bar{\eta}^B_b \mathscr{G}_{AB} = \bar{A}_{\mu ab}\ . \quad (13)$$

Likewise the normal vector in Eq.(9), it happens that the torsion vector, $A_{\mu ab}$, does not change under orthogonal perturbations. In geometric language, the presence of a torsion potential tilts the embedded family of submanifolds with respect to the normal vector $\eta^A_a$. If the bulk has certain killing vectors then $A_{\mu ab}$ transforms as the component of a gauge field under the group of isometries of the bulk [15, 28, 63]. It is worth noting that the gauge potential can only be present if the dimension of the bulk space is equal or greater than six ($n \geq 2$) in accordance with Eq.(13) since the torsion vector fields are antisymmetric under the exchange of extra coordinate $a$ and $b$. Thus, with the Eq.(10) and using the definition from Eq.(7), one obtains the perturbed metric and extrinsic curvature of the new geometry written as

$$g_{\mu\nu} = \bar{g}_{\mu\nu} - 2y^a \bar{k}_{\mu\nu a} + \delta y^a \delta y^b \left[ \bar{g}^{\sigma\rho} \bar{k}_{\mu\sigma a} \bar{k}_{\nu\rho b} + g^{cd} A_{\mu ca} A_{\nu db} \right], \quad (14)$$

and the related perturbed extrinsic curvature

$$k_{\mu\nu a} = \bar{k}_{\mu\nu a} - \delta y^b \left( g^{cd} A_{\mu ca} A_{\nu db} + \bar{g}^{\sigma\rho} \bar{k}_{\mu\sigma a} \bar{k}_{\nu\rho b} \right)\ . \quad (15)$$

Taking the derivative of Eq.(14) with respect to $y$ coordinate, one obtains Nash's deformation condition

$$\bar{k}_{\mu\nu a} = -\frac{1}{2} \frac{\partial \bar{g}_{\mu\nu}}{\partial y^a}\ . \quad (16)$$

The meaning of this expression is twofold. It can be realized in a pictorial view under the basic theory of curves, i.e., one gets a congruence of curves (or orbits) orthogonal to the embedded space $V_4$. Moreover, the parameter $y$ is time-like or not, and it is irrelevant the sign of its signature. A similar expression was obtained years later in the context of the ADM formulation by Choquet-Bruhat and York [64]. In fact, the physical interpretation of Eq.(16) means that it localizes the matter in the embedded space-time imposing on it a geometric confinement. In other words, it holds true for any perturbations resulting from $n$-parameter families of embedded submanifolds denoted by $y^a$, and the matter remains confined to the resulting perturbed metric that can bend and/or stretch without ripping the manifold (embedded space-time), which may be a valuable feature for a quantization process [17] and cosmology.

In addition, the integrability conditions for equations in Eq.(10) are given by the non-trivial components of the Riemann tensor of the embedding space expressed in the Gaussian frame $\{\mathscr{Z}^A_\mu, \eta^A_a\}$ known as the Gauss-Codazzi-Ricci equations. This guarantees to reconstruct the embedded geometry and to understand its properties from the dynamics of the four-dimensional embedded space-time. Consequently, we can define a Gaussian coordinate system in the new perturbed coordinates $\{\mathscr{Z}^A_{,\mu}, \eta^A_a\}$ in the vicinity of $V_4$ that allows us to write the metric of the bulk in such a way

$$\mathscr{G}_{AB} = \begin{pmatrix} g_{\mu\nu} + g^{ab} A_{\mu a} A_{\nu b} & A_{\mu a} \\ A_{\nu b} & g_{ab} \end{pmatrix}, \quad (17)$$

where the perturbed metric $g_{\mu\nu}$ is given by Eq.(14). The expression in Eq.(17) is the metric of the bulk with at least two extra-dimensions, i.e., $D \geq 6$. This resembles the non-Abelian Kaluza-Klein metric and the quantity $A_{\mu a}$ plays the role of the Yang-Mills potentials where $A_{\mu a} = x^b A_{\mu ab}$. We emphasize that for just one extra-dimension, the torsion vector does not exist and for two extra-dimensions it turns to the usual Maxwell field, which means that the non-Abelian part of $A_{\mu a}$ is lost in a six dimensional bulk. This means that the resulting force is the ordinary electromagnetic one in the case of two extra dimensions [18, 19, 28, 29].

As proposed in Refs.[15–17, 27, 30], one obtains the induced field covariant equations of motion taking Eq.(3) in the frame defined in Eq.(17) at background level. Thus, the background of a 4-D observer in the embedded space is set by the following equations

$$G_{\mu\nu} + Q_{\mu\nu} = 8\pi G T_{\mu\nu}\ , \quad (18)$$

where the quantity $T_{\mu\nu}$ denotes the stress energy tensors for ordinary intrinsic matter (including Yang-Mills fields). The second equation involves relations with extrinsic terms $\bar{k}_{\alpha\beta a}$ and $A_{\mu ab}$

$$\nabla^*_\nu \bar{k}_a - \nabla^*_\mu \bar{k}^\mu_{a\nu} = 8\pi G_N T_{a\nu}\ , \quad (19)$$

where the term $\nabla^*_\mu \bar{k}_{\alpha\beta a}$ denotes $\nabla^*_\mu \bar{k}_{\alpha\beta a} := \bar{k}_{\alpha\beta a;\mu} - A_{\mu ab} \bar{k}^b_{\alpha\beta}$ and the semicolon denotes the covariant derivative. Moreover, the third equation is denoted as

$$R + \bar{k}_{\mu\nu m} \bar{k}^{\mu\nu m} - \bar{k}_a \bar{k}^a = -16\pi G_N \eta_{ab} T_{ab}\ , \quad (20)$$

where $\eta_{ab} = \varepsilon_a \delta_{ab}$ with $\varepsilon_a = \pm 1$. The quantities $G$, $T_{a\nu}$, $T_{ab}$ denote the induced gravitational Newton's constant, the stress energy tensors projections of $T_{AB}$ on the cross and normal directions of the space-time, respectively.

Those set of equations are the results from the integrability conditions of the embedding given by the Gauss-Codazzi-Ricci equations. From the Nash-Green theorem, the solutions of these equations were obtained by a differentiable process [15, 16, 29]. The first of the two equations are known, respectively, by the gravi-tensor equation (a modified Einstein's equations by the appearance of the extrinsic curvature) as in Eq.(18) and the gravi-vector equation as in Eq.(19). In summary, they reflect the meaning of a dynamical embedding: the pseudo-Riemann curvature of the embedding space acts as a reference for the pseudo-Riemann curvature of the embedded space-time. Moreover, the projection of the Riemann tensor of the embedding space along the normal direction is given by the tangent variation of the extrinsic curvature as shown by Eq.(19) that is the trace of the Codazzi equations composed by the extrinsic terms $\bar{k}_{\alpha\beta a}, A_{\mu ab}$. The last equation is known as gravi-Scalar equation and serves as a constrain on the torsion vector fields $A_{\mu ab}$.

The quantity $Q_{\mu\nu}$ is denoted by

$$Q_{\mu\nu} = \bar{g}^{cd}\left(\bar{g}^{\rho\sigma}\bar{k}_{\mu\rho c}\bar{k}_{\nu\sigma d} - \bar{k}_{\mu\nu d}\bar{g}^{\alpha\beta}\bar{k}_{\alpha\beta c}\right) - \frac{1}{2}\left(\bar{k}_{\lambda\phi c}\bar{k}^{\lambda\phi}_{d}\,\bar{g}^{\alpha\beta}\bar{k}_{\alpha\beta d}\bar{g}^{\gamma\delta}\bar{k}_{\gamma\delta c}\right)\bar{g}_{\mu\nu}\,, \tag{21}$$

is an independently conserved quantity in the sense of Noether's theorem with $Q_{\mu\nu\,;\nu} = 0$. It means that this geometric new term does not exchange gravitational energy with ordinary matter and resembles the quintessence in the dark energy problem. The conservation of $Q_{\mu\nu}$ holds true for perturbed quantities of $g_{\mu\nu}$ and $k_{\mu\nu a}$.

## 2.2 The background cosmological model

To the present cosmological application, we consider a four-dimensional metric embedded in a five-dimensional bulk to make a proper comparison with the most of cosmological models in recent literature. In this framework, the set of field equations are simplified. The torsion vector $A_{\mu ab}$ does not exist in five-dimensions and Eq.(19) turns to a homogeneous equation and Eq.(20) provides only a relation of consistence between Ricci scalar and extrinsic scalar quantities (no a priori information is gained).

To obtain the embedded four-dimensional equations, one can take Eq.(18) written in the Gaussian frame embedding veilbein $\{\mathscr{X}^A_\mu, \eta^A_a\}$. This reference frame is composed by a regular and differentiable coordinate $\{\mathscr{X}^A_\mu\}$ and a unitary normal vector $\{\eta^A_a\}$. Accordingly, one can obtain the set of the embedded four-dimensional field equations

$$R_{\mu\nu} - \frac{1}{2}Rg_{\mu\nu} + Q_{\mu\nu} = 8\pi G T_{\mu\nu}\,, \tag{22}$$

$$k^{\rho}_{\mu;\rho} - h_{,\mu} = 0\,, \tag{23}$$

where the semi-colon denotes a covariant derivative. The $T_{\mu\nu}$ tensor is the four-dimensional energy-momentum tensor of a perfect fluid, expressed in co-moving coordinates as

$$T_{\mu\nu} = (p+\rho)U_\mu U_\nu + p\,g_{\mu\nu}, \quad U_\mu = \delta^4_\mu\,,$$

where $U_\mu$ is the co-moving four-velocity. Moreover, the deformation tensor $Q_{\mu\nu}$ is simplified and can given by

$$Q_{\mu\nu} = g^{\rho\sigma}k_{\mu\rho}k_{\nu\sigma} - k_{\mu\nu}H - \frac{1}{2}\left(K^2 - h^2\right)g_{\mu\nu}\,, \tag{24}$$

where we denote $h = g^{\mu\nu}k_{\mu\nu}$ and $h^2 = h.h$ is the mean curvature. The term $K^2 = k^{\mu\nu}k_{\mu\nu}$ denotes the related Gaussian curvature. As previously shown, it follows that $Q_{\mu\nu}$

$$Q^{\mu\nu}{}_{;\nu} = 0\,. \tag{25}$$

The related conservation equation for $T_{\mu\nu}$ is given by

$$\rho + 3H(\rho + p) = 0\,, \tag{26}$$

where $\rho$ and $p$ denote non-perturbed matter density and pressure, respectively. Moreover, we work with a spatially Friedman-Lemaître-Robertson-Walker (FLRW) geometry with line element expressed in coordinates $(r,\theta,\phi,t)$ in such a way

$$ds^2 = -dt^2 + a^2\left[dr^2 + f^2_\kappa(r)\left(d\theta^2 + \sin^2\theta d\varphi^2\right)\right]\,, \tag{27}$$

where $f(r)_\kappa = \sin r$, r,$\sinh r$. Since the FLRW geometry can be locally embedded in five-dimensions, it can be regarded as a four-dimensional hypersurface dynamically evolving in a flat five-dimensional bulk whose Riemann tensor $\mathscr{R}_{ABCD}$ is

$$\mathscr{R}_{ABCD} = 0\,, \tag{28}$$

where $\mathscr{G}_{AB}$ denotes the bulk metric components in arbitrary coordinates. Hence, with a flat dimensional bulk, concerning our cosmological applications, we are not considering the appearance of the cosmological constant $\Lambda$.

In the following, we summarize the background results obtained in previous works [16, 20]. Using Eq.(27), one obtains a solution for Eq.(23) that is given by

$$k_{ij} = \frac{b}{a^2}g_{ij},\ \ i,j = 1,2,3, \quad k_{44} = \frac{-1}{\dot{a}}\frac{d}{dt}\frac{b}{a},$$

where the extrinsic bending function $b(t) = k_{11}$ is function of time. The dot symbol denotes an ordinary time derivative. This arbitrariness follows from the confinement of the four-dimensional gauge fields, which produces the homogeneous equation as shown in Eq.(23).

Denoting the usual Hubble parameter by $H = \dot{a}/a$ and the extrinsic parameter $B = \dot{b}/b$, one obtains

$$k_{ij} = \frac{b}{a^2}g_{ij},\ \ k_{44} = -\frac{b}{a^2}\left(\frac{B}{H} - 1\right), \tag{29}$$

$$K^2 = \frac{b^2}{a^4}\left(\frac{B^2}{H^2} - 2\frac{B}{H} + 4\right),\ \ h = \frac{b}{a^2}\left(\frac{B}{H} + 2\right), \tag{30}$$

$$Q_{ij} = \frac{b^2}{a^4}\left(2\frac{B}{H} - 1\right)g_{ij},\ Q_{44} = -\frac{3b^2}{a^4}, \tag{31}$$

$$Q = -(K^2 - h^2) = \frac{6b^2}{a^4}\frac{B}{H}\,, \tag{32}$$

where in Eq.(31), we have denoted $i, j = 1..3$, with no sum in indices. For simplicity, we denote the expansion parameter as $a(t) = a$ and the bending function as $b(t) = b$.

Since the dynamics equations for the extrinsic curvature are not complete in five-dimensions, motivated by the lack of uniqueness of the function $b(t)$, and being the extrinsic curvature independent rank-2 field, one can derive the Einstein-Gupta equations [20, 65] in a form

$$\mathscr{F}_{\mu\nu} = 0\,, \tag{33}$$

where they are defined as a copy (concerning its structure) of the usual Riemannian geometry. Hence, once can define a "f-Riemann tensor"

$$\begin{aligned}\mathscr{F}_{\nu\alpha\lambda\mu} &= \partial_\alpha \Upsilon_{\mu\lambda\nu} - \partial_\lambda \Upsilon_{\mu\alpha\nu} + \Upsilon_{\alpha\sigma\mu}\Upsilon^{\sigma}_{\lambda\nu} - \Upsilon_{\lambda\sigma\mu}\Upsilon^{\sigma}_{\alpha\nu}\,,\\ \Upsilon_{\mu\nu\sigma} &= \frac{1}{2}\left(\partial_\mu f_{\sigma\nu} + \partial_\nu f_{\sigma\mu} - \partial_\sigma f_{\mu\nu}\right)\,,\\ \Upsilon_{\mu\nu}{}^{\lambda} &= f^{\lambda\sigma}\Upsilon_{\mu\nu\sigma}.\end{aligned}$$

that were constructed from a "connection" associated with $k_{\mu\nu}$ and

$$f_{\mu\nu} = \frac{2}{K}k_{\mu\nu}, \text{ and } f^{\mu\nu} = \frac{2}{K}k^{\mu\nu}\,, \tag{34}$$

in such a way that the normalization condition $f^{\mu\rho}f_{\rho\nu} = \delta^{\mu}_{\nu}$ applies.

### 2.3 The modified Friedmann equation

From the results of Eqs.(22), (23) and (25) by means of calculating $Q^{\mu}_{\mu,i} = 0$, the Friedmann equation modified by the extrinsic curvature can be written as

$$\left(\frac{\dot{a}}{a}\right)^2 = \frac{8}{3}\pi G\rho + \alpha_0 a^{2\beta_0-4}e^{\gamma^{\pm}(t)}\,, \tag{35}$$

where $\alpha_0$ denotes an integration constant originated from the influence of the extrinsic curvature. We point out that when $\alpha_0 \to 0$, we obtain the standard result of GR. Concerning the total energy $\rho$, we denote $\rho = \rho_{mat} + \rho_{rad}$, which is composed by the matter density $\rho_{mat}$ and the radiation energy density $\rho_{rad}$, respectively. The $\gamma$-exponent in the exponential function in Eq.(35) is defined as $\gamma^{\pm}(t) = \pm\sqrt{|4\eta_0 a^4 - 3|} \mp \sqrt{3}\arctan\left(\frac{\sqrt{3}}{3}\sqrt{|4\eta_0 a^4 - 3|}\right)$ and the relation of expansion scale factor with redshift is given by $a = \frac{1}{1+z}$. By means of background cosmography tests [23, 24, 26], it was shown that the parameter $\beta_0$ tunes the magnitude of the deceleration parameter $q(z)$ and the parameter $\eta_0$ adjusts the width of the transition phase redshift from a decelerating to accelerating phase. Moreover, we can write Friedman equations as

$$H(z) = H_0\sqrt{\Omega_m(z) + \Omega_{rad}(z) + \Omega_{ext}(z)e^{\pm\gamma(z)}}\,, \tag{36}$$

where $H(z)$ is the Hubble parameter in terms of redshift $z$ and $H_0$ is the current value of the Hubble constant. The matter density parameter is denoted by $\Omega_m(z) = \Omega^0_m(1+z)^3$, $\Omega_{rad}(z) = \Omega^0_{rad}(1+z)^4$ with $\Omega^0_{rad} = \Omega^0_m z_{eq}$ and the term $\Omega_{ext}(z) = \Omega^0_{ext}(1+z)^{4-2\beta_0}\gamma_0$ stands for the density parameter associated with the extrinsic curvature. The upper script "0" indicates the present value of any quantity. The equivalence number for the expansion factor $a_{eq}$ given by

$$a_{eq} = \frac{1}{1+z_{eq}} = \frac{1}{(1+2.5\times10^4\Omega_m h^2(T_{cmb}/2.7)^{-4})} \tag{37}$$

where $z_{eq}$ is the equivalence redshift. The CMB temperature we adopt the value $T_{cmb} = 2.7255K$ and the dimensionless Hubble parameter $h = 0.672$.

The complete form for Hubble parameter as in Eq.(36) has been investigated in a sequence of studies [20, 22–24, 26] but at perturbation level, the Hubble function in Eq.(36) is not continuous for any arbitrary redshift $z$ or, equivalently, for the expansion factor $a$. To obtain a stable solution, we analytically expand $H(a)$ by using a Mclaurin-Puiseux series with $\eta_0 \to 0$ for an asymptotic limit $a \to 0$ truncating at second order, i.e, $e^{\gamma(x(a))} \sim 1 + \frac{\sqrt{3}}{3}x(a)^{3/2} + \mathscr{O}(x^{5/2})$. Considering only the linear order, it gives roughly in terms of redshift $e^{\gamma(z)} \sim (z+1)^{-4}$. The convergence of $e^{\gamma(a)}$ is in compliance with the Walsh theorem on convergence of analytic approximations [66]. For a flat space, the current "extrinsic contribution" $\Omega^0_{ext}$ is given by the normalization condition for redshift at $z = 0$ that results in

$$\Omega^0_{ext} = \frac{2}{\eta_0}\left(1 - \Omega^0_m - \Omega^0_{rad}\right)\,. \tag{38}$$

Hence, we can write the dimensionless Hubble parameter $E(z) = \frac{H(z)}{H_0}$ as

$$\begin{aligned}E^2(z) = \Omega^0_m(1+z)^3 + \Omega^0_{rad}(1+z)^4 + \\ \left(1 - \Omega^0_m - \Omega^0_{rad}\right)(1+z)^{-2\beta_0}\,.\end{aligned} \tag{39}$$

To facilitate referencing, we call, for short, the proposed model as $\beta$-model.

## 3 Matter evolution equations in conformal Newtonian gauge

In longitudinal conformal Newtonian gauge, the metric in Eq.(27) is given by

$$ds^2 = a^2[(1+2\Phi)d\eta^2 - ((1-2\Psi)\delta_{ij}dx^i dx^j]\,, \tag{40}$$

where $\Phi = \Phi(\mathbf{x},\eta)$ and $\Psi = \Psi(\mathbf{x},\eta)$ denote the Newtonian potential and the Newtonian curvature, respectively. The conformal time $\eta$ is related with physical time as $dt = a(\eta)d\eta$.

The perturbed field equations of Eqs.(22) and (23) can be written as

$$\delta G^{\mu}_{\nu} = 8\pi G\delta T^{\mu}_{\nu} - \delta Q^{\mu}_{\nu}\,, \tag{41}$$

$$\delta k_{\mu\nu;\rho} = \delta k_{\mu\rho;\nu}\,. \tag{42}$$

To obtain the explicit form for perturbed field equations in Eqs.(41) and (42), we need to determine both perturbed

metric $\delta g_{\mu\nu}$ and perturbed extrinsic curvature $\delta k_{\mu\nu}$. Using the main result of the Nash-Green theorem [61, 62], one can use the relation

$$\delta g_{\mu\nu} = -2\bar{k}_{\mu\nu}\delta y \,, \tag{43}$$

where $\delta y$ denotes an infinitesimal displacement of the extra dimension $y$ in the bulk space.

The linear perturbations of a new geometry $g_{\mu\nu}$ is given by $g_{\mu\nu} = \bar{g}_{\mu\nu} + \delta g_{\mu\nu}$ that can be written as

$$g_{\mu\nu} = \bar{g}_{\mu\nu} - 2\delta y \bar{k}_{\mu\nu} \,, \tag{44}$$

and the related perturbed extrinsic curvature

$$k_{\mu\nu} = \bar{k}_{\mu\nu} - 2\delta y\, \bar{g}^{\sigma\rho}\bar{k}_{\mu\sigma}\bar{k}_{\nu\rho} \,, \tag{45}$$

where we can identify $\delta k_{\mu\nu} = \bar{g}^{\sigma\rho}\bar{k}_{\mu\sigma}\bar{k}_{\nu\rho}$. Using the Nash relation $\delta g_{\mu\nu} = -2\bar{k}_{\mu\nu}\delta y$, we obtain

$$\delta k_{\mu\nu} = \bar{g}^{\sigma\rho}\bar{k}_{\mu\sigma}\delta g_{\nu\rho} \,. \tag{46}$$

The perturbation of the deformation tensor $Q_{\mu\nu}$ can be made from its background form in Eq.(24) and the resulting $k_{\mu\nu}$ perturbations from Nash's fluctuations in Eq.(46). Thus, one obtains

$$\delta Q_{\mu\nu} = -\frac{3}{2}(K^2 - h^2)\delta g_{\mu\nu} \,. \tag{47}$$

It is worthy noting that due to the Nash fluctuations in Eq.(44), we notice that the Codazzi equations in Eq.(42) and the Einstein-Gupta equations in Eq.(33) are invariant under the Nash perturbations and are confined to the background (in the sense that they maintain the same background form). Then using the background relations in Eqs.(29), (30), (31), and (32), we can determine the components of $\delta Q_{\mu\nu}$

$$\delta Q^i_j = \gamma_0 a^{2\beta_0 - 2}\Psi\delta^i_j \,, \tag{48}$$
$$\delta Q^i_4 = 0 \,, \tag{49}$$
$$\delta Q^4_4 = \gamma_0 a^{2\beta_0 - 2}\Phi\delta^4_4 \,. \tag{50}$$

where $\gamma_0$ is a constant term that merges all integration constants and also carries an extrinsic curvature constant from integration of the bending function $b(t)$ which means that if $\gamma_0$ is zero, the usual GR configuration is restored once all terms originated from extrinsic curvature will vanish accordingly.

For a perturbed fluid with pressure $p$ and density $\rho$, one can write the perturbed components of the related stress-tensor

$$\delta T^4_4 = \delta\rho \,, \tag{51}$$
$$\delta T^4_i = \frac{1}{a}(\rho_0 + p_0)\delta u_{\|i} \,, \tag{52}$$
$$\delta T^i_j = -\delta p\, \delta^i_j \,, \tag{53}$$

where $\delta u_{\|i}$ denotes the tangent velocity potential and, $\rho_0$ and $p_0$ denote the non-perturbed components of density and pressure, respectively.

Moreover, we adopt the simplest condition for perturbations $\Psi = \Phi$ and obtain the following set of equations in the wave-number $k$-space of Fourier modes as

$$k^2\Phi_k + 3\mathscr{H}\left(\Phi_k' + \Phi_k\mathscr{H}\right) = -4\pi G a^2\delta\rho_k + 9\gamma_0 a^{2\beta_0}\Phi_k \,, \tag{54}$$

$$(a\Phi_k)' = -4\pi G a^2(\rho_0 + p_0)\theta \,, \tag{55}$$

$$\Phi_k'' + 3\mathscr{H}\Phi_k' + (\mathscr{H}^2 + 2\mathscr{H}')\Phi_k - 9\gamma_0 a^{2\beta_0}\Phi_k = 4\pi G a^2 c_s^2\delta\rho_k \,, \tag{56}$$

where the conformal Hubble parameter is $\mathscr{H} \equiv aH$, $c_s$ denotes the sound speed and $\theta = ik^j\delta u_{\|j}$ denotes the divergence of fluid velocity in $k$-space. Hence, from Eqs.(54), (55) and (56), one obtains the gravitational potential formula in $k$-space:

$$\Phi_k'' + 3(1 + c_s^2)\mathscr{H}\Phi_k' + \left[k^2c_s^2 + (1 + 3c_s^2)\mathscr{H}^2\right]\Phi_k = \gamma_0 a^{2\beta_0}(1 + c_s^2)\Phi_k - 2\mathscr{H}'\Phi_k \,. \tag{57}$$

As a matter of consistence, we point out when $\gamma_0 \to 0$ in Eq.(57), the standard GR correspondence is obtained. Thus, one recovers the subhorizon approximation with $k^2 >> \mathscr{H}^2$ or $k^2 >> a^2H^2$ and Eq.(57) turns the Newtonian formula $\Phi_k \sim \frac{\delta\rho_k}{k^2}$.

After a Fourier transform, we perform the definition of the "contrast" matter density $\delta_m \equiv \frac{\delta\rho}{\rho_0}$. For a pressureless matter and a null anisotropic matter stress, we use Eq.(54) and obtain a relation of $\Phi_k$ and $\delta_m$ given by

$$k^2\Phi_k = -4\pi G_{eff}a^2\rho_0\delta_m \,, \tag{58}$$

where $G_{eff}$ is the effective Newtonian constant and is given by

$$G_{eff}(a,k) = \frac{G}{1 - \frac{\gamma_0}{k^2}a^{2\beta_0}} \,, \tag{59}$$

where $G$ is the Newtonian gravitational constant.

The corresponding equation of evolution of the contrast matter density $\delta_m(\eta)$ in conformal longitudinal Newtonian frame can be written as

$$\delta_m'' + \mathscr{H}\delta_m' - 4\pi G_{eff}a^2\rho_0\delta_m = 0 \,, \tag{60}$$

where the prime symbols denote derivatives with respect to conformal time $\eta$. And, in terms of the expansion factor $a(t)$, we obtain the contrast matter density $\delta_m(a)$ accordingly

$$\ddot{\delta}_m(a) + \left(\frac{3}{a} + \frac{\dot{H}(a)}{H(a)}\right)\dot{\delta}_m(a) - \frac{3\Omega_{m0}G_{eff}/G}{2(H^2(a)/H_0^2)}\delta_m(a) = 0 \,, \tag{61}$$

where the dot symbols denote derivatives with respect to scale factor $a$.

## 4 Observational constraints: analysis and results

### 4.1 Cosmological data

The methodology used to handle the data relies on the Markov Chain Monte Carlo (MCMC) technique based on the Metropolis-Hasting algorithm. We perform our analysis using the joint likelihood of the CMB Planck 2015 data [1], Pantheon SnIa [40], the Hubble parameter as a function of redshift [41–46] and Baryonic Acoustic Oscillations (BAO) from points of the joint surveys 6dFGS [47], SDDS [48], BOSS CMASS [49], WiggleZ [50], MSG [51] and BOSS DR12 [52].

To apply our $\chi^2$-statistics, we have an overall 1121 data points. From each dataset, we have 1048 points from the Pantheon SNIa observations, 3 points from CMB, 9 of BAO, 36 points from Hubble parameter (with some clustering) and 25 points from growth data. We use the background parameter vectors $\{\Omega_{m0}, 100\Omega_b h^2, \beta_0, h, \sigma_8\}$ with the priors $\{(0.001,1),(0.001,0.08),(-0.3,1),(0.01,0.5),(0.1,1.8)\}$. Moreover, to implement the MCMC chains, the joint analysis is defined by the product of the particular likelihoods $\mathscr{L}$ for each data set

$$\mathscr{L}_{tot} = \mathscr{L}_{Pantheon}.\mathscr{L}_{BAO}.\mathscr{L}_{CMB}.\mathscr{L}_{H(z)}.\mathscr{L}_{Growth}\,, \tag{62}$$

and the sum of individual $\chi^2$ to get the related total $\chi^2$

$$\chi^2_{tot} = \chi^2_{Pantheon} + \chi^2_{BAO} + \chi^2_{CMB} + \chi^2_{H(z)} + \chi^2_{Growth}. \tag{63}$$

For the growth analysis, we use the $\sigma_8$ parameter that measures the growth of r.m.s fluctuations on the scale of $8h^{-1}$Mpc by defining the quantity

$$f\sigma_8(a) \equiv f(a).\sigma_8(a)\,, \tag{64}$$

where $f(a) = \frac{\ln\delta}{\ln a}$ is the growth rate and the growth factor $\delta(a)$. The data dependence from the fiducial cosmology and another cosmological survey must be compatibilized. It can be done by rescaling the growth-rate data by the ratio $r(z)$ of the Hubble parameter $H(z)$ and the angular distance $d_A(z)$ by the relation

$$r(z) = \frac{H(z)d_A(z)}{H_f(z)D_fA(z)}\,, \tag{65}$$

where the subscript "$f$" corresponds a quantity of fiducial cosmology. Moreover, the angular distance $d_A(z)$ is defined as

$$d_A(z) = \frac{c}{(1+z)}\int_z^0 \frac{1}{H(z')}dz'\,. \tag{66}$$

Likewise, the regulation of the $\chi^2$ statistics is given by

$$\chi^2(\Omega_{m0}, w, \sigma_8) = V^i C^{-1}_{ij} V_j\,, \tag{67}$$

where $V^i \equiv f\sigma_{8,i} - r(z_i)f\sigma_8(z_i, \Omega_{m0}, w, \sigma_8)$ denotes a set of vectors that go up to $ith$-datapoints at redshift $z_i$ for each $i = 1...N$. The term $N$ is the total number of datapoints of a related collection of data and from theoretical prediction we have the $f\sigma_{8,i}$ datapoints [32] as shown in Table 1.

The set of $C^{-1}_{ij}$ denotes the inverse covariance matrix with the covariant matrix $C_{ij}$ given by

$$C^{wigglez}_{ij} = 10^{-3}\begin{pmatrix} 6.400 & 2.570 & 0.000 \\ 2.570 & 3.969 & 2.540 \\ 0.000 & 2.540 & 5.184 \end{pmatrix} \tag{68}$$

and the resulting total matrix $C^{tot}_{ij}$

$$C^{tot}_{ij} = 10^{-3}\begin{pmatrix} \sigma_1^2 & 0 & 0 & ... \\ 0 & C^{wigglez}_{ij} & 0 & ... \\ 0 & 0 & ... & \sigma_N^2 \end{pmatrix} \tag{69}$$

where the set of $\sigma^2$'s denote the $N$-variances.

For the CMB data, we used the Planck2018 released [2] with $\chi^2$ statistics

$$\chi^2_{CMB} = X^T_{Planck2018} C^{-1}_{CMB} X_{Planck2018}\,, \tag{70}$$

where the covariant matrix for the parameters for $R, l_A, \Omega_{b0}h^2$ is given by

$$X_{Plankc2018} = \begin{pmatrix} R - 1.7502 \\ l_A - 301.471 \\ \omega_b - 0.02236 \end{pmatrix} \tag{71}$$

where $\omega_b = \Omega_{b0}h^2$. The quantities $R$ and $l_A$ are the shift parameters defined as the scale distance and acoustic scale, respectively, as

$$R = \frac{\sqrt{\Omega_{m0}}}{c} d_A(z_{CMB})(1+z_{CMB})\,, \tag{72}$$

$$l_A = \frac{\pi d_A(z_{CMB})(1+z_{CMB})}{r_s(z_{CMB})}\,, \tag{73}$$

where the angular distance $d_A$ is given by Eq.(66) and the related redshift at recombination $z_{cmb}$ is given by

$$z_{CMB} = 1048[1+0.00124(\Omega_b h^2)^{-0.738}][1+g_1(\Omega_{m0}h^2)^{g_2}]\,, \tag{74}$$

and the parameters $(g_1, g_2)$ are defined as

$$g_1 = \frac{0.0783(\Omega_b h^2)^{-0.238}}{1+39.5(\Omega_b h^2)^{0.763}};\;\; g_2 = \frac{0.560}{1+21.1(\Omega_b h^2)^{1.81}}\,. \tag{75}$$

The comoving sound horizon $r_s(z)$ is given by

$$r_s(z) = c\int_z^\infty \frac{c_s(z')}{H(z')}dz'\,, \tag{76}$$

and the related sound speed $c_s$

$$c_s(z) = \frac{1}{\sqrt{3(1+\bar{R}_b/(1+z))}}\,, \tag{77}$$

with $\bar{R}_b = 31500\Omega_{b0}h^2(T_{CMB}/2.7K)^{-4}$. Moreover, the inverse of the covariant matrix $C^{-1}_{CMB}$ for the parameters for $l_a, R, \Omega_{b0}h^2$ is given by $C^{-1}_{CMB} = \sigma_i\sigma_j C$, with $\sigma_i$ = (0.0046, 0.090, 0.00015) for the normalized covariance matrix given by

$$C = \begin{pmatrix} 1.00 & 0.46 & -0.66 \\ 0.46 & 1.00 & -0.37 \\ -0.66 & -0.33 & 1.00 \end{pmatrix} \tag{78}$$

**Table 1** A compilation of the Hubble function $H(z)$ data used in the current analysis [32]. The relatives error points are denoted by the $\sigma_H$ column.

| redshift | $H(z)$ | $\sigma_H$ | redshift | $H(z)$ | $\sigma_H$ |
|---|---|---|---|---|---|
| 0.07 | 69 | 19.6 | 0.57 | 96.8 | 3.4 |
| 0.09 | 69.0 | 12.0 | 0.593 | 104.0 | 13.0 |
| 0.12 | 68.6 | 26.2 | 0.60 | 87.9 | 6.1 |
| 0.12 | 68.6 | 26.2 | 0.68 | 92.0 | 8.0 |
| 0.179 | 75.0 | 4.0 | 0.73 | 97.3 | 7.0 |
| 0.199 | 75.0 | 5.0 | 0.781 | 105.0 | 12.0 |
| 0.2 | 72.9 | 29.6 | 0.875 | 125.0 | 17.0 |
| 0.27 | 77.0 | 14.0 | 0.88 | 90.0 | 40.0 |
| 0.28 | 88.8 | 36.6 | 0.9 | 117.0 | 23.0 |
| 0.35 | 82.7 | 8.4 | 1.037 | 154.0 | 20.0 |
| 0.352 | 83.0 | 14.0 | 1.3 | 168.0 | 17.0 |
| 0.3802 | 83.0 | 13.5 | 1.363 | 160.0 | 33.6 |
| 0.4 | 95.0 | 17.0 | 1.43 | 177.0 | 18.0 |
| 0.4004 | 77.0 | 10.2 | 1.53 | 140.0 | 14.0 |
| 0.4247 | 87.1 | 11.2 | 1.75 | 202.0 | 40.0 |
| 0.44 | 82.6 | 7.8 | 1.965 | 186.5 | 50.4 |
| 0.44497 | 92.8 | 12.9 | 2.34 | 222.0 | 7.0 |
| 0.4783 | 80.9 | 9.0 | | | |
| 0.48 9 | 7.0 | 62.0 | | | |

Similarly, in this paper, the BAO datasets are used from the conjunction of probes on SDSS [68–70], 6dFGS [71], IRAS [72, 73], 2MASS [72, 74], 2dFGRS [75], GAMA [76], BOSS[77], WiggleZ [78], Vipers [79], FastSound [80], BOSS Q [81] and additional points from the 2018 SSSD-IV [82–84]. The related $\chi^2$ statistics for WiggleZ is given by

$$\chi^2_{WiggleZ} = (\bar{A}_{obs} - \bar{A}_{th}) C^{-1}_{WiggleZ} (\bar{A}_{obs} - \bar{A}_{th})^T \,, \tag{79}$$

where $\bar{A}_{obs} = (0.447, 0.442, 0.424)$ denotes the set of observational values for data vectors at $z = (0.44, 0.60, 0.73)$ as compared with the theoretical predictions $\bar{A}_{th} = (z, p_i)$ which is defined as

$$\bar{A}_{th} = d_V(z) \frac{\sqrt{\Omega_{m0} H_0^2}}{cz} \,, \tag{80}$$

with the dilation scale

$$d_V(z) = \frac{1}{H_0} \left[ (1+z)^2 d_A(z)^2 \frac{cz}{E(z)} \right]^{1/3} . \tag{81}$$

Moreover, the inverse of the covariant matrix $C^{-1}_{WiggleZ}$

$$C^{-1}_{WiggleZ} = \begin{pmatrix} 1040.3 & -807.5 & 336.8 \\ -807.5 & 3720.3 & -1551.9 \\ 336.8 & -1551.9 & 2914.9 \end{pmatrix} . \tag{82}$$

Likewise, $\chi^2$ statistics on SDSS data is such as

$$\chi^2_{SDSS} = (\bar{d}_{obs} - \bar{d}_{th}) C^{-1}_{SDSS} (\bar{d}_{obs} - \bar{d}_{th})^T \,. \tag{83}$$

where $d_{obs}$ denotes the observable distance and $d_{th}$ is theoretical distance, respectively. The distance $d_{obs} = (0.1905, 0.1097)$ is calculated at $z = 0.2$ and $z = 0.35$, and $d_{th}$ is given by

$$\bar{d}_{th} = \frac{r_s(z_d)}{d_V(z)} \,, \tag{84}$$

where the related comoving sound horizon $r_s(z)$ and sound speed $c_s(z)$ were given previously by Eqs.(76) and (77), respectively. In addition, the drag redshift $z_{drag}$ is given by

$$z_{drag} = \frac{1291(\Omega_m h^2)^{0.251}}{1 + 0.659(\Omega_m h^2)^{0.828}} [1 + b_1 (\Omega_m h^2)^{b_2}] \,, \tag{85}$$

where $b_1 = 0.313(\Omega_m h^2)^{-0.419}[1 + 0.607(\Omega_m h^2)^{0.674}]$ and $b_2 = 0.238(\Omega_m h^2)^{0.223}$. The inverse of the covariant matrix $C^{-1}_{SDSS}$ is given by

$$C^{-1}_{SDSS} = \begin{pmatrix} 30124 & -17227 \\ -17227 & 86977 \end{pmatrix} . \tag{86}$$

All data is combined in the total $\chi^2_{BAO}$ as the sum of the individual $\chi^2$ of each dataset.

For the Pantheon supernova type Ia data the theoretical distance modulus $\mu_{th}(z)$ is given by

$$\mu_{th}(z) = 5 \log_{10}(d_L(z)) + \mu_0, \tag{87}$$

where $\mu_0 = 42.38 - 5 \log_{10} \mathbf{h}$. The luminosity distance $d_L$ related to Hubble expansion rate is given by

$$d_L(z|s, \mu_0) = (1+z) \int_0^z \frac{du}{E(u|s)} \,, \tag{88}$$

**Table 2** A summary of best-fit values of the background parameters calculated by using MCMC chains with the resulting $\chi^2$ values. The $\chi^2_{bf}$ denotes the $\chi^2$ best-fit values from MCMC and $\chi^2_{red}$ refers to reduced $\chi^2$ from the value of the minimum best-fit of $\chi^2$ and the related degree of freedom.

| Model | $\Omega_{m0}$ | $100\Omega_{b0}h^2$ | $h$ | $\sigma_8$ | model parameters | $\chi^2_{bf}$ |
|---|---|---|---|---|---|---|
| $\Lambda$CDM | 0.317± 0.006 | 2.234± 0.015 | 0.674± 0.004 | 0.758± 0.028 | $w=-1$ | 1087.82 |
| $w$CDM | 0.312± 0.008 | 2.233± 0.015 | 0.679± 0.008 | 0.760± 0.028 | $w=-1.023\pm 0.033$ | 1087.40 |
| $\beta$-model | 0.316± 0.006 | 2.233± 0.014 | 0.674± 0.004 | 0.761± 0.028 | $\beta_0$=0.001± 0.009 | 1087.86 |

**Table 3** A summary of mean values of background parameters calculated by using MCMC chains with the main parameters.

| Model | $\Omega_{m0}$ | $100\Omega_{b0}h^2$ | $h$ | $\sigma_8$ | model parameters |
|---|---|---|---|---|---|
| $\Lambda$CDM | 0.316± 0.006 | 2.235± 0.015 | 0.674± 0.004 | 0.761± 0.028 | $w=-1$ |
| $w$CDM | 0.312± 0.007 | 2.234± 0.015 | 0.680± 0.008 | 0.759± 0.028 | $w=-0.993\pm 0.027$ |
| $\beta$-model | 0.3180± 0.006 | 2.236± 0.014 | 0.672± 0.004 | 0.761± 0.029 | $\beta_0$=0.010± 0.008 |

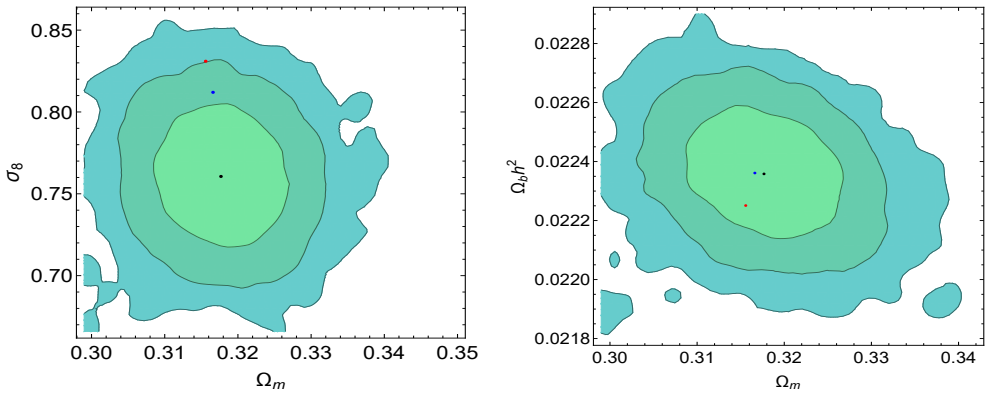


**Fig. 1** Contour regions at 1-$\sigma$, 2-$\sigma$ and 3-$\sigma$ at 68.3%, 95.4% and 99.7% C.L, respectively, in the $(\sigma_8 - \Omega_m)$ and $(100\Omega_{b0}h^2 - \Omega_m)$ planes. The black points represent the mean values of the parameters in the MCMC chains. The blue point denotes the relate Planck2018 data and the red points denote the CMB Planck2015 data in respect to the related quantities.

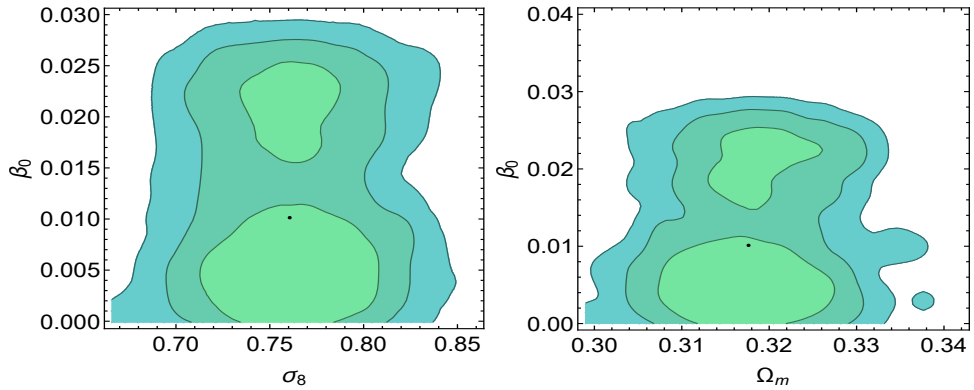


**Fig. 2** Marginalized $\beta_0$ with $\sigma_8$ and $\Omega_m$ parameters in the left and right panels, respectively.

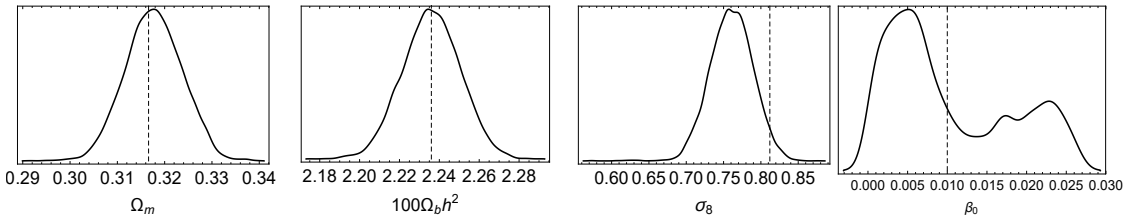


**Fig. 3** One-dimensional PDF likelihood of the cosmological parameters for the cosmological parameters in the $\beta$-model used in this study. The vertical dashed lines indicate the CMB Planck 2018 values. The panel also shows the degeneracies for the $\beta_0$ values.

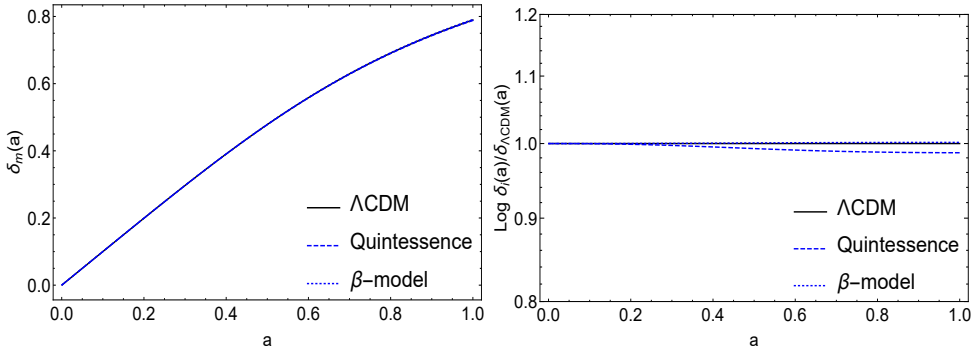


**Fig. 4** Numerical solution of Matter density evolution. The right panel shows the comparisons of $\Lambda$CDM, GR quintessence and $\beta$-model with the mean values in Table 3. The left panel shows in logarithm scale the comparison with these models by the ratio $\delta_i/\delta_{m\Lambda CDM}$.

where $s$ denotes the model parameters. As a prior, we adopt the density parameter value of visible baryonic matter $\Omega_{b0} = 2.236/100\mathbf{h}^2$. Accordingly, the $\chi^2$ statistics is

$$\chi^2_{SnIa}(s|\mu_0) = \sum_{i=1}^{n} \frac{\left[\mu_{th,i}(s,\mu_0|z_i) - \mu_{obs,i}(z_i)\right]}{\sigma^2_{\mu i}} , \qquad (89)$$

where $n = 1048$ is the number of events of the Pantheon SNIa data [40], the distance modulus obtained from observations is denoted by $\mu_{obs,i}(z_i)$, and $\sigma_{\mu i}$ is the total uncertainty of the observational data.

## 4.2 Results and discussions

In Fig.(1), we present the obtained $3\sigma$-contour plots. The black points mark the obtained mean values from MCMC chains. The left panel presents a $(\sigma - \Omega_m)$ contour that shows a mild (reduced) tension at 2-$\sigma$ (blue points mark CMB Planck2018 data) in comparison with the 3-$\sigma$ tension form CMB Planck2015 (red points) between low redshift data $H(z)$ and the Planck probe. In the right panel, it is shown the $(100\Omega_{b0}h^2 - \Omega_m)$ plane that pinpoints a mild increase of tension in the $100\Omega_{b0}h^2$ values in Planck2015 but an interesting better accommodation of the baryonic luminous matter parameter with the values from Planck2018 data within the 1-$\sigma$ contour. An important matter is shown in Fig.(3) that exhibits the PDF behaviour of the main parameters. The degeneracies found in the marginalization of $\beta_0$ and the mild degeneracy in the related $\sigma_8$ values may decrease the obtained 2-$\sigma$ tension in $\sigma_8$ contour. Moreover, in Fig.(2), we present the marginalization of $\beta_0$-parameter in respect to the $\sigma_8$ and $\Omega_m$ parameters where the mean values (black points) are settled in 1-$\sigma$ region in both cases.

In Fig.(4) is shown the behaviour of the growth evolution of the $\beta$-model (Eq.(61)) in comparison with $\Lambda$CDM and GR quintessence. The adopted values were from the mean values in Table 3 from MCMC chains. In the left panel, it is shown that the resulting curves from the models are indistinguishable. A relative comparison between the models is shown the right panel a close proximity of the behaviour of growth of $\Lambda$CDM and the $\beta$-model with almost indistinguishable slight upper values that favor the curves of the latter. For the GR quintessence, it presents lower values as compared to the previous ones starting from the early universe around $a \sim 0.2$. In the Fig.(5) we obtain the percentage relative difference between the aforementioned model in what concerns the evolution of Hubble function. In the left panel, it shows in linear scale that the percentage difference between $\beta$-model with $\Lambda$CDM and GR quintessence reaches no more than 1% in early times and tends to close equivalence in present time, with mild fluctuations in the range a$\sim 0.6 - 0.8$. Those fluctuations are clearer in the central panel with the spikes in the curves due to the degeneracies on the parameter that leads to a mild signature on the baryonic luminous matter. Moreover, to reinforce the phenomenological distances between the models, we apply the Om(z) diagnosis [55] as a null test, by using the formula

$$Om(z) = \frac{E(z)^2 - 1}{(1+z)^3 - 1} . \qquad (90)$$

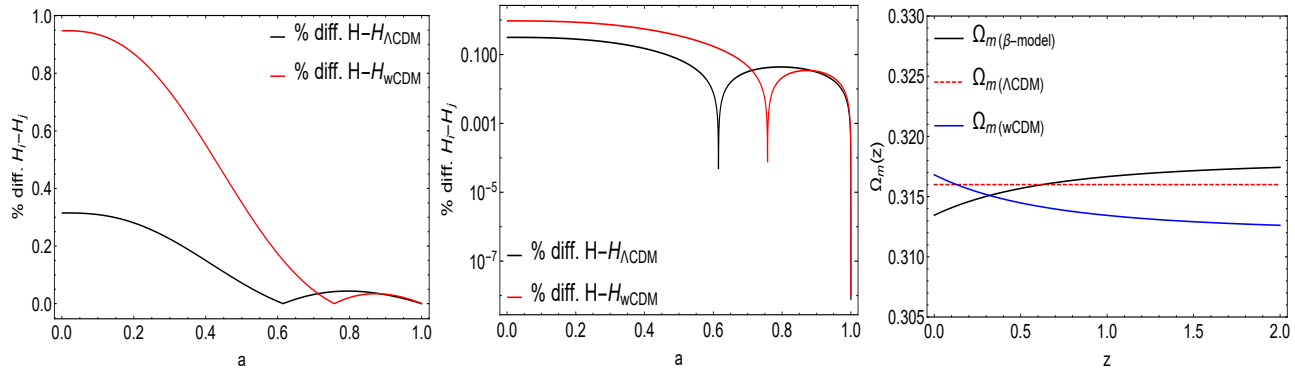


**Fig. 5** The percentage relative difference $\%\text{diff}(H-H_j)$ between the $\beta$-models, $\Lambda$CDM and GR quintessence for the mean values in Table 3 in linear (left panel) and logarithm (central panel) scales. In the right panel, it is shown Om(z) diagnosis.

**Table 4** A summary of the obtained values of AIC for the studied models. The $\Lambda$CDM model is adopted as a reference.

| Model | $AIC$ | $\Delta AIC$ | Evidence against the model |
|---|---|---|---|
| $\Lambda$CDM | 1095.86 | 0 | null |
| $w$CDM | 1097.45 | 1.60 | weak |
| $\beta$-model | 1097.91 | 2.06 | substantially weak |

The right panel shows in the dashed red line the same values for Om(z) for any redshift as expected for $\Lambda$CDM. The black and blue solid lines indicate Om(z) values higher ($\beta$-model) and lower (GR quintessence), respectively, like that of evolving dark energy models. We expect that a large percentage difference can be obtained with higher orders of Mclaurin-Puiseux series that provides an interesting control on growth density.

Another useful tool to analyse the model comparisons refers to the level of statistical correlation between such models. Adopting the errors being as Gaussian, we use AIC systematic to classify the fit-to-data for small samples sizes [67, 85]

$$AIC = \chi^2_{bf} + 2k\frac{2k(k+1)}{N-k-1}\,, \tag{91}$$

where $\chi^2_{bf}$ is the best-fit $\chi^2$ of the model, $k$ represents the number of the free parameters and $N$ is the number of the data point in the adopted dataset. The difference $|\Delta AIC| = AIC_{model\,2} - AIC_{model\,1}$ obeys the Jeffreys' scale [86] that measures the intensity of tension between two competing models due to the lost information from the related fitting. In general, the preferred model is that one with lesser values for AIC. In comparison, higher values of AIC denote a higher statistical distance and may indicate a statistically disfavoring model. In Jeffreys' scale for $|\Delta AIC \leq 2|$ tells that the models are statistically consistent with a certain good level of empirical support. For $4 < \Delta AIC < 7$ indicates a positive tension against the model with a higher value of AIC. For $|\Delta AIC \geq 10|$ defines a strong empirical evidence against the model with a higher AIC. Accordingly, we have obtained the AIC and $\Delta AIC$ values shown in Table 4 that indicates some weak evidence against $\beta$-model with a $\Delta AIC$ roughly $\sim 2$. This result reinforces the previous one and leads to the conclusion that the $\beta$-model favors statistical consistency with $\Lambda$CDM and $w$CDM models at present time with mild fluctuation at perturbation level.

## 5 Remarks

In this paper, we discussed the dark energy problem with a proposal of a geometric model in a search of explanation of the accelerated expansion. By construction, we used the Nash-Green theorem to propose a geometric model with a resulting modified Friedman equation from the influence of the extrinsic curvature thought as a complement to Einstein's gravity. From background level, an asymptotic solution valid in the range $a = [0,1]$ was obtained using a Mclaurin-Puiseux series of the Hubble function $H(z)$ due to the fact the parameter $\eta_0 \to 0$. At perturbation level, we obtained the perturbed equations in the longitudinal Newtonian gauge. From the MCMC analysis, we obtained the resulting contours from the analysis on $(\sigma_8 - \Omega_m)$ plane with a 3-$\sigma$ reduction on $\sigma_8$ tension. In the $(100\Omega_{b0}h^2) - \Omega_m$ plane, we obtained a reduction of the $\sigma$-distance within the 1-$\sigma$ contour as compared with the Planck2015 and Planck2018 data, in which the $\beta$-model is well accommodated to the latter dataset. The related PDF 1-dimensional plot shows the degeneracies on the parameters and may improve the aforementioned $\sigma_8$ tension. Such situation does not happen in the $\Lambda$CDM and $w$CDM usual contexts. From numerical solu-

tions on growth and $H(z)$ evolutions, it was shown a certain compatibility between the $\beta$-model with $\Lambda$CDM and $w$CDM models with a percentage difference up to 1% at early times. This small difference appears to be limited only to the second Maclaurin-Puiseux expansion order. Moreover, we applied the AIC classifiers that favour the $\Lambda$CDM model but with a statistical compatibility with $\beta$-model with $\Delta AIC$ roughly at $\sim 2$. As future prospects, we intend to investigate that how the $\beta$-model may inflict changes in the Integrated Sachs–Wolfe (ISW) contribution in comparison with the one as predicted to $\Lambda$CDM with a lower peak of the second CMB peak. Also, to investigate the behaviour of the viscosity parameter and growth index rate resulting from the $\beta$-model in a search of a more realistic context. This process is in due course and will be reported elsewhere.

**Acknowledgements** The author thanks Federal University of Latin-American Integration for financial support from Edital PRPPG 110 (17/09/2018) and Fundação Araucária/PR for the Grant CP15/2017-P&D 67/2019.

## References


1. P. A. R. Ade et al., (Planck Collaboration), Astron. Astrophys. **594**, A13 (2016).
2. N. Aghanim et al., (Planck Collaboration), Planck 2018 results. VI. Cosmological Parameters, ArXiv:1807.06209, (2018).
3. R. J. Nemiroff, R. Joshi, B. R. Atla, JCAP**06**, 006 (2015).
4. B. Santos, A. A. Coley, C. N. Devi, J. S. Alcaniz, JCAP**02**, 047 (2017).
5. P. Kumar, C. P. Singh, Astrophys Space Sci. **362**, 52 (2017).
6. H. E. S. Velten, R. F. vom Marttens, W. Zimdahl, Eur. Phys. J. C**74**, 11, 3160 (2014).
7. J. Sultana, Mon. Not. Roy. Astron. Soc. **457**(1), 212-216 (2016).
8. N. Sivanandam, Phys. Rev. D**87**, 083514 (2016).
9. K. Nozari, N. Behrouz, N. Rashidi, Adv. High En.Phys., Article ID 569702, (2014).
10. N. Arkani-Hamed, S. Dimopoulos, G. Dvali, Phys. Lett., B**429**, 263 (1998).
11. L. Randall, Sundrum R., Phys. Rev. Lett. **83**, 3370 (1999).
12. L. Randall, Sundrum R., Phys. Rev. Lett., **83**, 4690 (1999).
13. G. Dvali, G. Gabadadze, M. Porrati, Phys. Lett.B**485**, 208-214 (2000).
14. R. A. Battye, B. Carter, Phys. Lett. B**509**, 331 (2001).
15. M. D. Maia, E. M. Monte, Phys. Lett. A**297**, 2, 9-19 (2002).
16. M. D. Maia, E. M. Monte, J. M. F. Maia, J. S. Alcaniz, Class.Quantum Grav.**22**, 1623 (2005).
17. M. D. Maia, N. Silva, M. C. B. Fernandes, JHEP**04**, 047 (2007).
18. M. Heydari-Fard M., Sepangi H. R., Phys.Lett.B**649**, 1-11 (2007).
19. S. Jalalzadeh, M. Mehrnia, H. R. Sepangi., Class.Quant.Grav.**26**,155007 (2009).
20. M. D. Maia, A. J. S. Capistrano, J. S. Alcaniz, E. M. Monte, Gen. Rel. Grav.**10**, 2685 (2011).
21. A. Ranjbar, H. R. Sepangi, S.. Shahidi, Ann. Phys.**327**, 3170-3181 (2012).
22. A. J. S. Capistrano, L. A. Cabral, Ann. Phys.**384**, 64-83 (2014).
23. A. J. S. Capistrano, Montl. Not. Roy. Soc. **448**, 1232-1239 (2015).
24. A. J. S. Capistrano, L. A. Cabral, Class. Quantum Grav. **33**, 245006 (2016).
25. A. J. S. Capistrano, A. C. Gutiérrez-Piñeres, S. C. Ulhoa, R. G. G. Amorim, Ann. Phys.**380**, 106–120 (2017).
26. A. J. S. Capistrano, Ann. Phys. (Berlin), 1700232 (2017).
27. A.J. S. Capistrano, Phys. Rev. D**100**, 064049-1 (2019).
28. S. Jalalzadeh, B. Vakili, H. R. Sepangi, Phys. Scr.**76**, 122 (2007).
29. M. D. Maia, Inter. Journ. Mod. Phys. A**31**, 1641010 (2016). D. C. N. Cunha, M. D. Maia, Massive Kaluza-Klein Gravity, [Arxiv: 1310.8525v1]
30. S. Jalalzadeh, T. Rostami, Inter. Journ. Mod. Phys. D**24**, 4, 1550027 (2015).
31. Eva-Maria Mueller et al., Mon. Not. Roy. Astron. Soc. **475**, 2, 2122 (2018).
32. S. Nesseris, G. Pantazis, L. Perivolaropoulos, Phys. Rev. D **96**, 2, 023542 (2017).
33. L. Kazantzidis, L.Perivolaropoulos, Phys. Rev. D **97**, 103503 (2018).
34. R. Gannouji, L. Kazantzidis, L. Perivolaropoulos, D. Polarski, Phys. Rev. D**98**, 104044 (2018).
35. E. Di Valentino, E. Linder A. Melchiorri, Phys. Rev. D**97**, 043528 (2018).
36. G. Lambiase, S. Mohanty, A. Narang, P. Parashari, Eur. Phys. J. C**79**, 14 (2019).
37. S. Bahamonde, K. F. Dialektopoulos, J. L. Said, Phys. Rev. D**100**, 064018 (2019).
38. C. A. Luna, S. Basilakos, S. Nesseris, Phys. Rev. D**98**, 023516 (2018).
39. R. Arjona, W. Cardona, S. Nesseris, Phys. Rev. D**99**, 043516 (2019).
40. D. M. Scolnic et al., Astrophys. J.**859**, 101 (2018).
41. C. Zhang, H. Zhang, S. Yuan, T. J. Zhang, Y.-C. Sun, Res. Astron. Astrophys. **14**, 1221 (2014).

42. D. Stern, R. Jimenez, L. Verde, M. Kamionkowski, S. A. Stanford, JCAP**1002**, 008 (2010).
43. M. Moresco et al., JCAP**1208**, 006 (2012).
44. C.H. Chuang, Y. Wang, Mon. Not. Roy. Astron. Soc.**435**, 255 (2013).
45. M. Moresco, Mon. Not. Roy. Astron. Soc.**450**, L16 (2015).
46. T. Delubac et al. (BOSS collaboration), Astron. Astrophys.**574**, A59 (2015).
47. F. Beutler et al., Mon. Not. Roy. Astron. Soc.**416**, 3017 (2011).
48. L. Anderson et al., (BOSS collaboration), Mon. Not. Roy. Astron. Soc.**441**, 24 (2014).
49. X. Xu, N. Padmanabhan, D. J. Eisenstein, K. T. Mehta, A. J. Cuesta, Mon. Not. Roy. Astron. Soc.**427**, 2146 (2012).
50. C. Blake et al., Mon. Not. Roy. Astron. Soc.**425**, 405 (2012).
51. A. J. Ross et al., Mon. Not. Roy. Astron.Soc.**449**, 835 (2015).
52. H. Gil-Marín et al., Mon. Not. Roy. Astron. Soc.**460**, 4210 (2016).
53. R. R. Caldwell, R. Dave, P. J. Steinhardt, Phys. Rev. Lett.**80**, 1582 (2018).
54. B. Ratra, P. J. E. Peebles, Phys. Rev. D**37**, 3406 (1988).
55. V. Sahni, A. Shafieloo, A. A. Starobinsky, Phys. Rev. D**78**, 103502 (2008).
56. H. Akaike, IEEE Transactions of Automatic Control**19**, 716 (1974).
57. G. Schwarz, Ann. Statist.**5**, 461 (1978).
58. S. K. Donaldson, Contemporary Mathematics (AMS)**35**, 201 (1984).
59. C. H. Taubes, Contemporary Mathematics (AMS)**35**, 493 (1984).
60. C. S. Lim, Prog. Theor. Exp. Phys., 02A101 (2014).
61. J. Nash, Ann. Maths.**63**, 20 (1956).
62. R. Greene, Memoirs Amer. Math. Soc.**97** (1970).
63. B. Holdom B., *the cosmological constant and the embedded universe*, Standford preprint ITP-744, (1983).
64. Y. Choquet-Bruhat, J. Jr York , Mathematics of Gravitation, Warsaw: Institute of Mathematics, Polish Academy of Sciences, (1997).
65. S. N. Gupta, Phys. Rev.**96**, 6 (1954).
66. J. L. Walsh, Trans. Amer. Math. Sot.**30**, 307-332 (1928).
67. N. Sugiura, Communications in Statistics A**7**, 13 (1978).
68. L. Samushia, W. J. Percival, A. Raccanelli, Monthly Not. R. Astron. Soc.**420**, 2102 (2012).
69. C. Howlett, A. Ross, L. Samushia, W. Percival, M. Manera, Monthly Not. R. Astron. Soc.**449**, 1, 848 (2015).
70. M. Feix, A. Nusser, E. Branchini, Phys. Rev. Lett. **115**, 1, 011301 (2015).
71. D. Huterer, D. Shafer, D. Scolnic, F. Schmidt, JCAP**1705**, 05, 015 (2017).
72. M. J. Hudson, S. J. Turnbull, Astrophys. J.**751**, L30 (2013).
73. S. J. Turnbull, et al., Monthly Not. R. Astron. Soc. **420**, 447 (2012).
74. M. Davis et al., Monthly Not. R. Astron. Soc. **413**, 2906 (2011).
75. Y. S. Song, W. J. Percival, JCAP**0910**, 004 (2009).
76. C. Blake et al., Monthly Not. R. Astron. Soc.**436**, 3089 (2013).
77. A. G. Sanchez et al., Monthly Not. R. Astron. Soc. **440**, 3, 2692 (2014).
78. C. Blake et al., Monthly Not. R. Astron. Soc.**425**, 405 (2012).
79. A. Pezzotta et al., Astron. Astrophys.**604**, A33 (2017).
80. T. Okumura et al., Publ. Astron. Soc. Jap.**68**, 3, 38 (2016).
81. P. Zarrouk et al., Monthly Not. R. Astron. Soc.**477**, 2, 1639 (2018).
82. H. Gil-Marín et al., Monthly Not. R. Astron. Soc.**477**, 2, 1604-1638 (2018).
83. J. Hou et al., Monthly Not. R. Astron. Soc.**480**, 2, 2521-2534 (2018).
84. Gong-Bo Zhao et al., Monthly Not. R. Astron. Soc.**482**, 3, 3497-3513 (2019).
85. A. R. Liddle, Mon. Not. R. Astron. Soc.**377**, L74–L78 (2007).
86. H. Jeffreys, Theory of Probability, 3rd edn. Oxford Univ. Press, Oxford (1961).